*Structural Engineering and Mechanics, Vol. 36, No. 3 (2010) 321-341*
DOI: http://dx.doi.org/10.12989/sem.2010.36.3.321 

# Development of a nonlinear seismic response capacity spectrum method for intake towers of dams

Leonardo Cocco[1a], Luis E. Suárez*[2] and Enrique E. Matheu[3b]

[1]*Department of Structures, School of Engineering, National University of Cordoba, Córdoba 5000, Argentina*
[2]*Department of Civil Engineering and Surveying, University of Puerto Rico, Mayagüez, Puerto Rico 00681-9000*
[3]*Office of Infrastructure Protection, US Department of Homeland Security, Arlington, Virginia 22201, USA*

*(Received November 9, 2007, Accepted June 17, 2010)*

**Abstract.** The seismic-induced failure of a dam could have catastrophic consequences associated with the sudden release of the impounded reservoir. Depending on the severity of the seismic hazard, the characteristics and size of the dam-reservoir system, preventing such a failure scenario could be a problem of critical importance. In many cases, the release of water is controlled through a reinforced-concrete intake tower. This paper describes the application of a static nonlinear procedure known as the Capacity Spectrum Method (CSM) to evaluate the structural integrity of intake towers subject to seismic ground motion. Three variants of the CSM are considered: a multimodal pushover scheme, which uses the idea proposed by Chopra and Goel (2002); an adaptive pushover variant, in which the change in the stiffness of the structure is considered; and a combination of both approaches. The effects caused by the water surrounding the intake tower, as well as any water contained inside the hollow structure, are accounted for by added hydrodynamic masses. A typical structure is used as a case study, and the accuracy of the CSM analyses is assessed with time history analyses performed using commercial and structural analysis programs developed in Matlab.

**Keywords:** intake towers; capacity spectrum method; dams; nonlinear static analysis; seismic behavior.

## 1. Introduction

Intake towers are typically thick-walled hollow reinforced-concrete structures that contain water discharge control equipment. A previous examination of a representative intake tower inventory such as the one under the responsibility of the U.S. Army Corps of Engineers (USACE) indicated that these are generally lightly-reinforced structures (Dove and Matheu 2005). To account for the demand imposed by earthquakes in those structures located in seismically active regions, it was common practice to use static forces determined by using a simple seismic coefficient approach. Once the forces were evaluated, it was standard practice to design the towers using approximate

*Corresponding author, Professor, E-mail: luis.suarez3@upr.edu
[a]Instructor
[b]Chief

formulae such as those developed for reinforced concrete chimneys (ACI Committee 1995). These methods are currently regarded as out-of-date and inaccurate. Furthermore, even for those intake towers that were originally analyzed and designed with more refined approaches, in several cases the associated seismic hazard has been upgraded due to new seismological studies that have identified previously unknown seismic faults near the site.

All these factors contribute to the fact that many of the existing intake towers could potentially be seismically deficient and thus prone to failure during a strong earthquake. Obviously, any structural failure or damage is always an undesirable event, but in the case of intake towers the situation is more critical. These structures play an important role in controlling the release of the impounded water. This controlled release may be required if the dam suffers severe damage during an earthquake. Moreover, the failure of an intake tower during an earthquake could also cause critical disruptions in the provision of fresh water or in the generation of electricity.

The seismic analysis of intake towers for design purposes is currently done by means of response-spectrum based procedures. Because these approaches assume that the structure behaves in a linear fashion, a response reduction factor is typically introduced to reduce the design forces due to increased damping and period change caused by allowed inelastic behavior, by system redundancy, hysteretic behavior and overstrength. By judiciously selecting an appropriate reduction factor, along with proper detailing, the structure should have the sufficient integrity, strength, and toughness to resist collapse in severe seismic events. Although this is currently the standard approach for seismic design of intake structures, it has some shortcomings when the goal is to evaluate the seismic performance of an existing structure by predicting the amount of earthquake-induced damage to be experienced. The analyst faced with this task has two alternatives, as described next.

The most suitable method for evaluation of the actual seismic performance of an intake tower would be an inelastic time history analysis. This type of approach can predict with sufficient reliability the forces and cumulative deformation demands in every element of the structural system (Krawinkler and Seneviratna 1997). The structural engineering field has experienced notable advances in the last three decades, paralleling the progress in computer hardware and software; however, inelastic time history approaches are not a practical alternative for a large inventory of structures.

Therefore, faster and simpler procedures are sought for systematic application to a large number of relatively simple structural configurations. Nonlinear static procedures could be used with advantage for this purpose. The Capacity Spectrum Method (CSM) is one of these simpler procedures, and it is the methodology proposed in this study for seismic evaluation of intake towers. For a complete explanation of this method and a description of its application to the rehabilitation of buildings, the reader is referred to ATC-40 (1996).

To the best of the authors' knowledge, the Capacity Spectrum Method has not been previously applied to intake towers. The applications reported in the literature are predominantly focused on building structures, although the method has also been successfully applied to bridges (Paraskeva *et al.* 2006, Isakovic and Fischinger 2006, Casarotti and Pinho 2007, Lupoi *et al*. 2007). One of the most important differences between the applications of the CSM to intake towers and to buildings is the presence of water inside and outside the towers. The effect of water in the seismic response of hydraulic structures is usually taken into account by means of added hydrodynamic masses (Goyal and Chopra 1989). The previous versions of the CSM do not include this feature and thus the method will be appropriately modified so that it can be applied to semi-submerged structures.

The classical CSM is based on the assumption that the fundamental mode of the structure is sufficient to represent its dynamic behavior. This is usually accurate enough for the analysis of regular buildings. However, for the response spectrum analysis of intake towers at least two modes should be considered (USACE 2003). It is reasonable to expect that the same requirement may also be necessary for a nonlinear analysis. Therefore, an extension of the CSM, referred to as the multimodal CSM, will be considered for the seismic analysis of intake towers.

Another version of the CSM, known as the adaptive CSM, will be studied. This approach has been proposed by a few authors (see for instance, Casarotti and Pinho 2007, Kalkan and Kunnath 2006) to account for the changes in the mode shapes and other dynamic properties of the structure as it enters the inelastic range. It has been shown that this enhanced implementation of the CSM is capable of producing more accurate results in the case of building structures. The validity of this approach will be examined for intake towers.

## 2. The capacity spectrum method

The Capacity Spectrum Method was originally introduced in 1975 as a procedure for the rapid evaluation of the seismic vulnerability of buildings (Freeman *et al*. 1975). This method has gone through several stages of development and upgrade (Freeman 1978, 1987, Mahaney *et al*. 1993, Freeman 1992, Gupta and Kunnath 2000, Antoniou and Pinho 2004a, b). However, the fundamental procedure is based on a simple concept, namely a comparison of the capacity of the structure against the seismic demand. Graphically, this can be described by superposing a curve representing the capacity of the structure, known as the capacity spectrum, with another curve representing the seismic demand, the ground response spectrum. The point where the curves intersect is called the performance point and its coordinates represent an estimate of the approximate inelastic response of the structure to the specified seismic demand.

The first step in the application of this method is to estimate the pushover curve (or capacity curve) of the structure, i.e., the relationship between a parameter representing the level of lateral force applied to the structure and a characteristic displacement representing the resulting displaced configuration of the structure. Typically, the base shear, $V_b$, and the displacement at a selected point of the structure (usually at the top, $\Delta_{top}$) are selected as the relevant parameters. There are two different ways to obtain the capacity curve: one is by "pushing" the structure until a specified displacement is attained at a characteristic point. This is done by imposing incremental displacements, and obtaining at each step the base shear and the characteristic displacement. This method is called the displacement-controlled approach. The other method to determine the pushover curve, referred to as the force-controlled approach, is based on the application of a lateral load with a certain pattern that is gradually incremented in magnitude while keeping the shape fixed, until a specified base shear is reached. The base shear and characteristic displacement are calculated and plotted at each step of the loading process.

One important attribute of the latter method is the proposed lateral load pattern. The applied lateral loads represent the forces acting on the structure when it is excited by an earthquake. Therefore, the load pattern must be as similar as possible to the inertial forces generated by the imposed ground motions. There are several spatial distributions proposed for these lateral forces: uniform in height, proportional to the tributary mass at each level, with a pattern described by the static method of the seismic codes, or proportional to the first mode (Pyle and Morris 2001). Probably the most popular lateral load pattern is the fundamental mode distribution. In such a distribution, the magnitude of the lateral forces is proportional to the elastic first mode shape and the mass matrix of the structure. This is the distribution adopted in this paper to implement the original CSM. This study uses an additional pattern to define the lateral loading, which is known as the adaptive lateral force distribution. In this case, the force distribution varies with the change in the structural deflected shape that takes place after yielding.

Regardless of the load patterns and control methods chosen to determine the pushover curve, this curve must be changed to a new format by changing the two axes. The original pushover curve ($V_b$ vs. $\Delta_{top}$) is converted to a spectral acceleration versus spectral displacement format ($S_A$ vs. $S_D$). To accomplish this transformation, it is assumed that the response of the structure is governed by a single mode, the mode corresponding to the fundamental period. The equations to transform the base shear and top displacement are

$$S_A = \frac{V_b/W_T}{\alpha_1}; \quad S_D = \frac{\Delta_{top}}{\gamma_1 \phi_{top,1}} \tag{1}$$

where $W_T$ is the total weight of the structure, $\gamma_1$ is the modal participation factor of the first mode, $\phi_{top,1}$ is the modal displacement of the first mode, calculated at the node and direction where the displacement $\Delta_{top}$ is defined, and $\alpha_1$ is the modal mass coefficient of the first mode. The pushover curve drawn in the new format is referred to as the "capacity spectrum". Although the Eqs. (1) are concerned with the first mode shape of the structure, they can be applied to any mode shape that governs the response.

When the structure behaves in a linear fashion, the demand is commonly represented by a 5% damping ratio response spectrum. In the CSM, the seismic demand is represented by a reduced ground response spectrum, which represents an inelastic response spectrum. Whether one intends to use an elastic or inelastic response spectrum, it must be changed from the conventional spectral acceleration versus natural period $T$ format to the spectral acceleration versus spectral displacement format. The curve graphed in the new format is referred to as the "demand spectrum". In order to do this, the abscissa of the new spectrum must be defined with the following equation.

$$S_D = \frac{T_2}{4\pi^2} S_A \tag{2}$$

The definition of the inelastic spectrum is one of the few still controversial issues of the CSM. Some authors (Fajfar 1999, Fajfar and Dolsek 2001) proposed using inelastic spectra that are based on constant ductility factors. The ATC-40 report (1996) proposes a different approach. The inelastic response spectra are represented by a set of spectra reduced for higher damping values. Each curve corresponds to an effective damping ratio, $\xi_{ef}$. This damping ratio takes into account the additional damping due to the hysteresis loop formed when the structure experiences cyclic deformations beyond the yield point. In addition, the possible degradation of the hysteresis loop is accounted for by a modification factor, $\kappa$. To define the effective damping ratio, the hysteresis loop must be idealized somehow. If it is assumed that the loop can be represented by a parallelogram, it can be shown that $\xi_{ef}$ is

$$\xi_{ef} = \xi_e + \kappa \frac{2}{\pi} \frac{a_y d_p - a_p d_y}{a_p d_p} \tag{3}$$

where $\xi_e$ is the elastic damping ratio (usually assumed to be 0.05), $d_y$ and $a_y$ are the displacement and acceleration at the yield point, and $d_p$ and $a_p$ are the peak (instantaneous) spectral displacement and acceleration. The set of higher damping spectra can be defined by applying the reduction factors based on the well known study by Newmark and Hall (1982). Using these factors, a set of reduced demand curves are obtained.

The capacity spectrum will intersect more than one reduced response spectrum, and the performance point is defined by the intersection of the capacity and demand curves for which the effective damping is exactly the same. By using Eq. (3), each point on the capacity spectrum can be associated with an effective damping ratio, $\xi_{ef}$, and the performance point can be determined by a search algorithm. It is clear that this point depends on the level of inelastic deformation, as shown in Eq. (3).

## 3. Shortcomings and enhancements of the CSM

Although the CSM is regarded as sufficiently accurate for design and seismic assessment, it is realized that it has some limitations. The most important limitations are the application of the loads following an invariant pattern, the disregard of the influence of the higher modes, and the use of an equivalent viscous damping ratio. Recognizing the fact that invariant load patterns are not compatible with the progressive yielding of the structure, several authors (Bracci *et al*. 1997, Gupta and Kunnath 2000, Antoniou and Pinho 2004a, b, Cocco 2004) have proposed adaptive load patterns for the CSM. The basic procedure consists of using the "instantaneous" mode shape of the structure as the pattern to apply the loads, as well as the updated modal properties to change the pushover curve to capacity spectrum. There is relatively recent and innovative method which is relevant to mention here. The method was proposed by Casarotti and Pinho and the details are provided in their reference; just the main ideas are described next. To construct the capacity curve, an equivalent system displacement using the current deformed shape at each step and the lumped masses is determined. In fact, this displacement is the inverse of a modal participation factor in which the deformed shape is used instead of a mode shape. Then the spectral acceleration in the vertical axis is defined as the ratio between the base shear and an effective system mass and the acceleration of gravity. The effective mass is defined in a similar way as the modal mass except that the current deform patter is used instead of the mode shape. These properties are updated at each step of the process which gives the adaptive character to the method.

The original CSM is applicable for structures that vibrate in their fundamental mode. However, the original CSM was recently revisited to overcome this limitation by incorporating response contributions associated with higher modes (Chopra and Goel 2002). In particular, the study evaluates the application of the multimodal CSM proposed by Chopra and Goel (2002) to the problem of seismic analysis of intake towers.

It can be shown that for a linear case the CSM reduces to the Response Spectrum Method (RSM). Therefore, if a series of pushover analyses is carried out for each mode of a linear structure and the responses are combined with a modal combination rule, the results obtained will be the same as those obtained with the RSM. Moreover, the differences between the results of an RSM and a linear time history analysis are usually small. Based on these concepts, Chopra and Goel (2002) proposed to apply the original CSM for each important mode of the structure. In this multimodal CSM, a performance point is obtained only if a performance point is found for each mode considered. The performance point for the structure is given by the combination of the modal performance points, which can be conducted by means of any appropriate combination rule such as the well-known

SRSS rule. Chopra and Goel (2002) demonstrated that when this methodology is applied to buildings, the results compare quite well with those from nonlinear time history analyses. Therefore, it is expected that the method could also be appropriate for intake towers.

Another modification of the original CSM is considered in this study by replacing the standard viscous damping ratio model with the hysteretic damping model proposed by Kowalsky (1994). This model is based on the Takeda hysteretic model, which considers the stiffness degradation and energy dissipation in a vibration cycle of the inelastic system by means of an equivalent linear system. As demonstrated by Lin and Chang (2003), this damping model is able to provide more accurate results. The expression of the damping ratio for the Kowalsky model is

$$\xi_{eq} = \xi_o + \frac{1}{\pi}\left[1 - \mu^n\left(\frac{1-\alpha}{\alpha} + \alpha\right)\right] \tag{4}$$

where $\alpha$ is the strain hardening ratio, $\mu$ is the ductility ratio, $\xi_o$ is the inherent damping, and the exponent $n$ is a stiffness degradation factor. It was suggested to use a value $n$ = 0 for steel structures and $n$ = 0.5 for reinforced concrete structures (Lin and Chang 2003). A value of 0.5 was used for applications to lightly reinforced concrete intake towers.

## 4. Effects of the surrounding and inside water

There are two major approaches to account for the influence of the water on the dynamic response of the structural system. The most sophisticated procedure involves the modeling of the fluid domain by means of finite or boundary elements. A much simpler approach consists of incorporating the hydrodynamic effects by using added masses. This is the approach adopted in this study. In particular, the procedure developed by Goyal and Chopra (1989) is used to define the required added masses. Although most real intake towers are non-prismatic and the Goyal and Chopra procedure is strictly valid for uniform towers, it is possible to obtain a good approximation by considering that the tower is formed by several segments with constant sections.

For a uniform tower with circular cross-section, the added hydrodynamic mass corresponding to the outside water can be determined in closed form by solving the Laplace equation for the water domain (Liaw and Chopra 1974). The normalized distribution of added hydrodynamic mass along the height of the tower $m_a^o(z)$ is given by

$$\frac{m_a^o(z)}{m_\infty^o} = \frac{16H_o}{\pi^2 r_o}\sum_{m=1}^{\infty}\frac{(-1)^{m-1}}{(2m-1)^2}E_m(\alpha_m r_o/H_o)\cos(\alpha_m z/H_o) \tag{5}$$

where the superscript $o$ refers to “outside”, $z$ is the distance above the base of the tower, $H_o$ is the depth of the surrounding water, $\alpha_m = (2m-1)\pi/2$, and $m_\infty^o$ represents the added hydrodynamic mass corresponding to an infinitely long uniform tower with the same cross section. The function $E_m(\alpha_m r_o/H_o)$ is defined as follows

$$E_m(\alpha_m r_o/H_o) = \frac{K_1(\alpha_m r_o/H_o)}{K_0(\alpha_m r_o/H_o) + K_2(\alpha_m r_o/H_o)} \tag{6}$$

where $K_n$ denotes the modified Bessel function of order $n$ of the second kind. For a tower with a circular cross section, $m_\infty^o = \rho_w \pi r_o^2$ where $\rho_w$ is the mass density of the water and $r_o$ is the radius of the outside surface of the tower. For non-circular cross sections, $m_\infty^o$ can be obtained from a table prepared by Goyal and Chopra (1989).

For towers with arbitrary cross sections there are no analytical solutions of the Laplace equation. Goyal and Chopra (1989) solved this problem by first showing that the normalized hydrodynamic mass for a uniform tower of arbitrary cross-section is essentially the same as that for an equivalent elliptical tower. They characterized the cross sections in terms of the plan-dimensions ratio, $\tilde{a}_o/\tilde{b}_o$, and the slenderness ratio, $H_o/\tilde{a}_o$, of the equivalent elliptical tower as follows

$$\frac{H_o}{\tilde{a}_o} = \frac{H_o}{\sqrt{\frac{A_o}{\pi}}}\sqrt{\frac{b_o}{a_o}}; \quad \frac{\tilde{a}_o}{\tilde{b}_o} = \frac{a_o}{b_o} \tag{7}$$

where $A_o$ is the enclosed cross section of the outside surface of the actual tower, and $2a_o$ and $2b_o$ are the cross-section dimensions perpendicular and parallel, respectively, to the direction of the ground motion. Hence, the normalized added hydrodynamic mass for a uniform tower of arbitrary cross-section could be readily determined if the normalized added hydrodynamic mass were available for towers of elliptical cross section for a practical range of values of $a_o/b_o$ and $H_o/a_o$. However, this methodology would require a large number of graphs and tables. A more convenient approach is to replace the uniform elliptical tower by an equivalent circular cylindrical tower. To this end, Goyal and Chopra determined the ratio $\tilde{r}_o/H_o$ of the equivalent circular cylindrical tower as a function of the ratios $a_o/b_o$ and $a_o/H_o$ of an elliptical tower. This ratio can be obtained from a graph prepared by Goyal and Chopra (1989), a simplified version of which is presented in Fig. 1.

Although the true relationship between $\tilde{r}_o/H_o$ and $a_o/H_o$ is not linear, for the purpose of the present work it was assumed so in Fig. 1. The error introduced by this approximation is not significant. Once the properties of the equivalent circular tower are estimated, the hydrodynamic added mass can be calculated from Eq. (5) with $m_\infty^o$ determined from Table 1 of Goyal and Chopra (1989).

The calculation of the added mass for the inside water is based on similar concepts. First, using the cross-sectional dimensions of the actual tower, the geometry ratios of the equivalent uniform elliptical tower are determined as follows

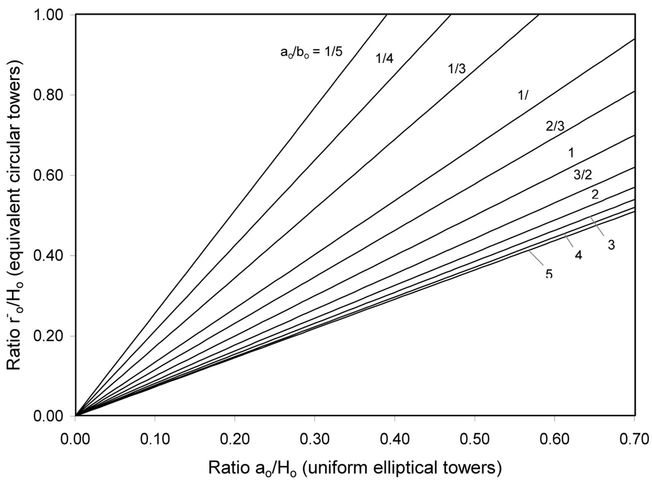


Fig. 1 Dimensions of the equivalent circular cylindrical towers (Goyal and Chopra 1989)

Table 1 Material properties used for analysis of example tower

| | |
|---|---|
| (a) Concrete Material Properties | |
| Modulus of Elasticity ($E_c$) | 21,525.43 MPa |
| Shear Modulus ($G$) | 8,986.93 MPa |
| Poisson's Ratio ($\nu$) | 0.20 |
| Compressive Strength ($f_c'$) | 20.68 MPa |
| (b) Steel Material Properties | |
| Modulus of Elasticity ($E_s$) | 199,947.95 MPa |
| Yield Strength ($f_y$) | 413.69 MPa |
| Ultimate Strain | 5.00% |

$$\frac{H_i}{\tilde{a}_i} = \frac{H_i}{\sqrt{\frac{A_i}{\pi}}}\sqrt{\frac{b_i}{a_i}}; \quad \frac{\tilde{a}_i}{\tilde{b}_i} = \frac{a_i}{b_i} \tag{8}$$

where $A_i$, $2a_i$, and $2b_i$ represent the interior cross-sectional area and dimensions perpendicular and parallel, respectively, to the direction of the ground motion; and $H_i$ is the depth of the inside water. Next, the slenderness ratio $\tilde{r}_i/H_i$ of the equivalent circular cylindrical tower should be determined as it was done for the outside water. However, Goyal and Chopra (1989) found that in this case the relationship between $a_i/H_i$ and $\tilde{r}_i/H_i$ is exactly linear and thus the radius $\tilde{r}_i$ can be simply calculated as

$$\tilde{r}_i = \sqrt{\frac{A_i b_i}{\pi a_i}} \tag{9}$$

Finally, the normalized added hydrodynamic mass corresponding to the water inside the tower, $m_a^i(z)$, can be calculated with the analytical solution of the Laplace equation for a circular cylindrical tower

$$\frac{m_a^i(z)}{m_\infty^i} = \frac{16H_i}{\pi^2 r_i}\sum_{m=1}^{\infty}\frac{(-1)^{m-1}}{(2m-1)^2}D_m(\alpha_m r_i/H_i)\cos(\alpha_m z/H_i) \tag{10}$$

where the superscript "*i*" refers to "interior" and $m_\infty^i = \rho_w \pi r_i^2$. The function $D_m(\alpha_m r_i/H_i)$ is defined as follows

$$D_m(\alpha_m r_i/H_i) = \frac{I_1(\alpha_m r_i/H_i)}{I_0(\alpha_m r_i/H_i)+I_2(\alpha_m r_i/H_i)} \tag{11}$$

and $I_n$ denotes the modified Bessel functions of order $n$ of the first kind.

## 5. Application of the CSM for seismic evaluation of intake towers

To present an example of the application of the CSM for seismic evaluation of intake towers, a representative structure was selected. This particular structure has served as an example in the manual for structural design and evaluation of outlet works of the U.S. Army Corps of Engineers (2003). This document is designated as Engineer Manual (EM) 1110-2-2400, and the case study under consideration, which is described in Appendix C of the manual, centers on an intake tower typical of those in the USACE inventory of intake structures.

### *5.1 Numerical model of the example structure*

The reinforced concrete tower is non-prismatic and is composed of five segments with different sections. It is capped at the top by a 0.61 m thick concrete slab and has a 1.83 m thick slab at the base. The elevation views of the tower in two orthogonal planes are shown in Fig. 2. The tower was discretized using twelve beam elements. This is the same discretization used in the example in the USACE EM 1110-2-2400 (2003). The discrete model is shown in Fig. 3, and the material properties considered for the analyses are listed in Table 1.

The geometrical properties of the twelve elements (numbered from the top to the bottom) used to model the tower are presented in Table 2. Except for elements 1 and 12, all the others have hollow rectangular sections. Elements 1 and 12 represent the solid slabs at the top and bottom of the tower, respectively. As part of the structural evaluation, it is necessary to determine the location of the critical section(s) in order to use a nonlinear element in this section(s). Because free-standing towers are subjected to lateral forces induced by seismic actions, the most critical sections are usually located near the base. In this case, and because of the massive characteristics of the bottom slab, the

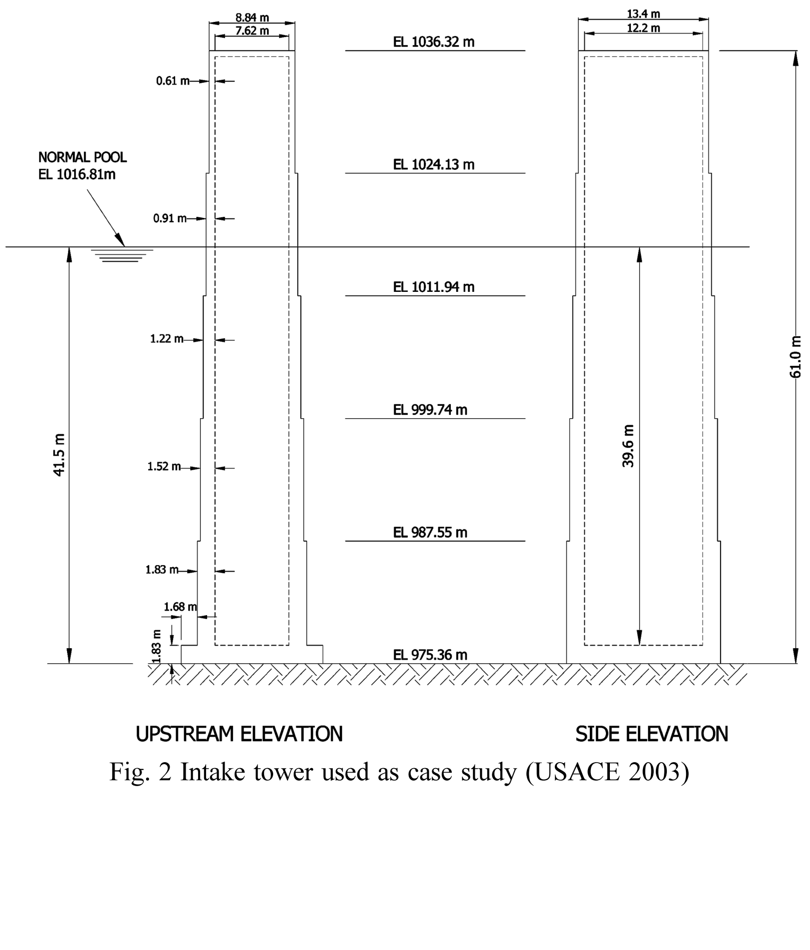


Fig. 2 Intake tower used as case study (USACE 2003)

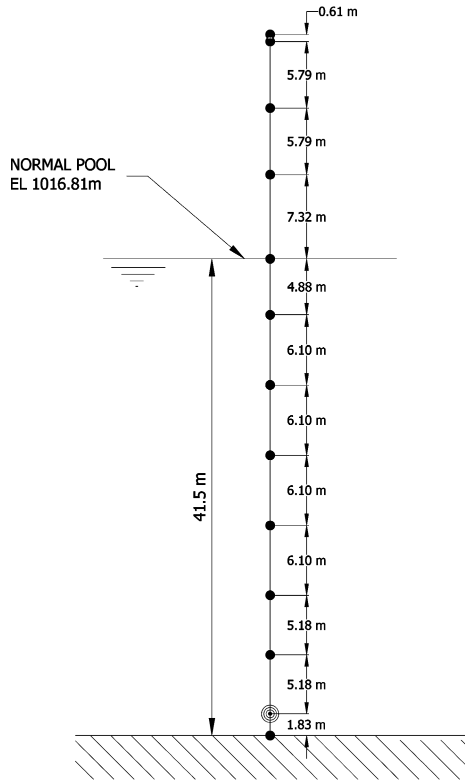


Fig. 3 Frame model of example tower

Table 2 Sectional properties of example tower

| Element | Length [m] | Area [m$^2$] | Inertia [m$^4$] | Shear Factor |
|---|---|---|---|---|
| 1 | 0.61 | 118.54 | 1777 | 1.20 |
| 2 | 5.79 | 25.64 | 626 | 1.64 |
| 3 | 5.79 | 25.64 | 626 | 1.64 |
| 4 | 7.32 | 39.02 | 965 | 1.67 |
| 5 | 4.88 | 39.02 | 965 | 1.67 |
| 6 | 6.10 | 52.77 | 1324 | 1.69 |
| 7 | 6.10 | 52.77 | 1324 | 1.69 |
| 8 | 6.10 | 66.89 | 1703 | 1.72 |
| 9 | 6.10 | 66.89 | 1703 | 1.72 |
| 10 | 5.18 | 81.38 | 2104 | 1.74 |
| 11 | 5.18 | 81.38 | 2104 | 1.74 |
| 12 | 1.83 | 214.05 | 3818 | 1.20 |

critical section is located at the transition between the base slab and the first hollow segment of the tower. In a general case, all sections must be evaluated until the actual critical sections are identified.

The geometry and material properties of the critical section are used to calculate the corresponding moment-curvature relationship. The nonlinearity of the structure will be introduced in the model by means of a rotational spring. Therefore, a moment-rotation curve is needed which can be determined based on the moment-curvature relationship and an appropriate plastic hinge length through which the curvature is integrated in order to obtain the rotation. Based on this moment-rotation curve, the behavior of the critical section under monotonic loading can be effectively modeled by a nonlinear rotational spring.

Based on previous studies performed by Dove and Matheu (2005) on lightly reinforced intake towers, an appropriate moment-rotation curve for the critical section can be obtained by considering a plastic hinge length, $l_p$, estimated by the following expressions

$$l_p = \frac{c_u}{\varepsilon_u} \tag{12}$$

where $c_u$ represents the ultimate crack width and $\varepsilon_u$ is the ultimate strain of the reinforcing steel. The value of the ultimate crack width $c_u$ in mm can be estimated as $c_u = 1.17 + 24.68\varepsilon_u + 0.312d_b$, where $d_b$ is the rebar diameter in mm. The expression was obtained from a series of laboratory experiments and it is valid strictly for lightly reinforced hollow rectangular cross sections (Dove and Matheu 2005).

Fig. 4 displays the resulting moment-rotation relationship for the critical section of the example tower, corresponding to a plastic hinge length $l_p = 273$ mm obtained using $\varepsilon_u = 0.05$ and $d_b = 36$. To facilitate the analysis, a bilinear approximation is adopted for the moment-rotation curve. In addition, the first linear segment of the moment-rotation curve in the figure will be disregarded. This segment represents the initial (elastic) stiffness of the rotational spring, but this stiffness is already included in the stiffness matrix of the frame element. Once yielding occurs, the nonlinear segment of the rotational spring is activated and it begins to affect the behavior of the element.

To complete the input data for the seismic analysis it is necessary to determine the corresponding hydrodynamic added masses. The cross-sectional dimensions that are required to account for the water outside and inside the tower, $(a_o, b_o)$ and $(a_i, b_i)$, respectively, are shown in Table 3 for the different segments along the height. Only those segments located below the water level are used to determine the added masses. Considering the normal pool elevation, the level of the surrounding water was taken equal to $H_o = 41.5$ m (measured with respect to the tower base) and for the water inside the

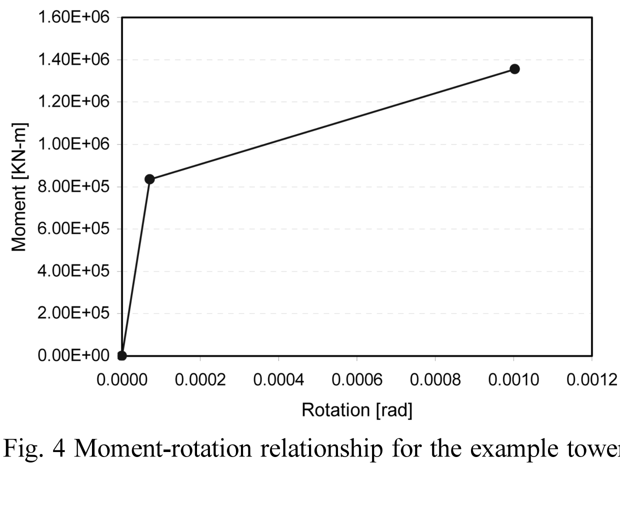


Fig. 4 Moment-rotation relationship for the example tower

Table 3 Cross-sectional properties for added hydrodynamic mass calculation

| Element | $a_o$ [m] | $b_o$ [m] | $a_i$ [m] | $b_i$ [m] |
|---|---|---|---|---|
| 1 | 8.84 | 13.41 | 0.00 | 0.00 |
| 2 | 8.84 | 13.41 | 7.62 | 12.19 |
| 3 | 8.84 | 13.41 | 7.62 | 12.19 |
| 4 | 9.54 | 13.72 | 7.62 | 11.90 |
| 5 | 9.54 | 13.72 | 7.62 | 11.90 |
| 6 | 10.06 | 14.02 | 7.62 | 11.58 |
| 7 | 10.06 | 14.02 | 7.62 | 11.58 |
| 8 | 10.67 | 14.33 | 7.62 | 11.29 |
| 9 | 10.67 | 14.33 | 7.62 | 11.29 |
| 10 | 11.28 | 14.63 | 7.62 | 10.97 |
| 11 | 11.28 | 14.63 | 7.62 | 10.97 |
| 12 | 14.63 | 14.63 | 0.00 | 0.00 |

tower, the level $H_i$ was set equal to 39.6 m (measured with respect to the top of the base slab).

### 5.2 Seismic demand

The seismic input must be prescribed by means of an appropriate design spectrum. The response spectrum for the example in Appendix C of EM 1110-2-2400 was defined based on the UBC 97 code. Assuming that the soil profile corresponds to rock conditions (type $S_B$), and that the structure is located in seismic zone 2B according to the UBC 97, the corresponding peak ground acceleration should be $C_a = 0.20$. However, the following parameters must be selected to match the spectrum with that shown in the USACE manual EM 1110-2-2400: $C_a = 0.25, C_v = 0.31, T_a = 0.10$ sec, and $T_s = 0.10$ sec. The resulting response spectrum to be used for all the CSM-based analyses of the example tower is displayed in Fig. 5.

This study will compare the CSM results with those predicted using nonlinear time history

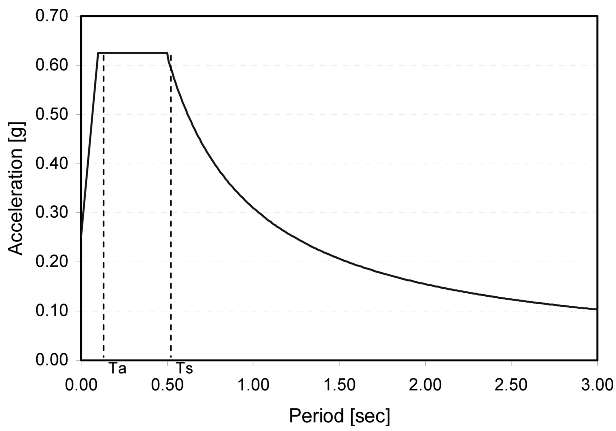


Fig. 5 Design response spectrum for example tower

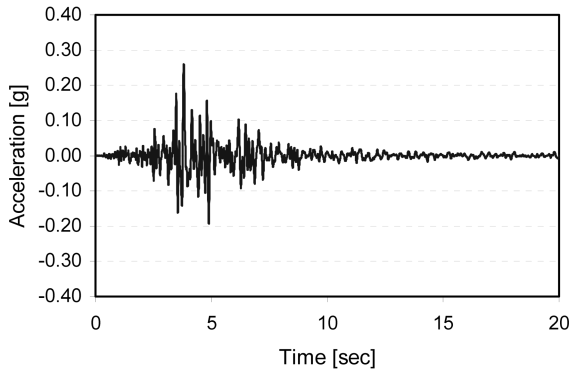


Fig. 6 1976 Friuli earthquake accelerogram

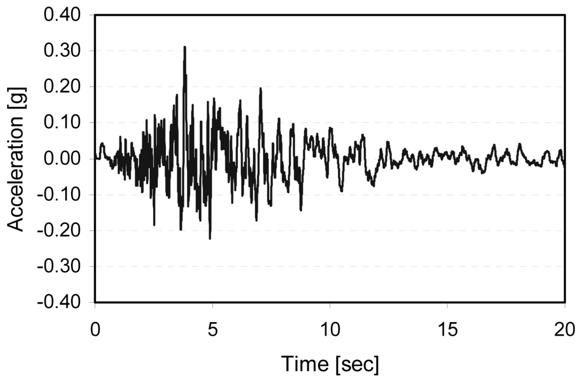


Fig. 7 Spectrum-compatible accelerogram used for nonlinear time-history analysis

analyses. For these analyses, the seismic input must be defined in terms of a ground acceleration time history. Furthermore, to compare the results obtained with the two approaches, the ground motion time history must be compatible with the spectrum shown in Fig. 5. A procedure to generate artificial records based on the wavelet transform (Suarez and Montejo 2005) is applied to generate a particular spectrum-compatible accelerogram. This technique is based on the appropriate modification of a seed acceleration time history of a real earthquake record. For the analysis of an actual structure, the seed accelerogram should be selected among earthquakes generated by similar faults as those present in the region, recorded at similar epicentral distances and soil conditions. However, for the present case the record of the 1976 Friuli, Italy earthquake shown in Fig. 6 was arbitrarily selected. Because of the modification introduced during the process, the final displacement and velocity of the resulting accelerogram are no longer zero, even though the original record satisfied these conditions. An appropriate correction of the accelerogram was performed using a technique described by Suarez and Montejo (2007). The corrected record used for the nonlinear time history analysis of the example tower is shown in Fig. 7.

### 5.3 Application of the conventional and multimodal CSM

To compute the nonlinear seismic response of the example tower, the first approach considered in this study is the standard CSM assuming empty reservoir conditions. Fig. 8 shows the pushover curve obtained by applying a load pattern proportional to the first mode shape. The two different stiffnesses, before and after yielding, are clearly depicted in the pushover curve of Fig. 8. The analysis was stopped when the ultimate rotation (0.001 radians) at the critical section was attained.

The pushover curve can be transformed into a capacity spectrum as explained in Section 3 and is shown in Fig. 9. The figure also shows the 5%-damping elastic response spectrum in the acceleration-displacement format. The variable damping response spectrum (representing the seismic demand for different levels of effective damping) is displayed in the same Fig. 9, along with the point of intersection between the capacity and demand spectra. The coordinates $(S_A, S_D)$ and $(V_b, \Delta_{top})$ of the performance point are shown in the column "first mode" of Table 4.

Next, the tower is analyzed by applying the multimodal version of the CSM as proposed by Chopra and Goel (2002). Since only the first and second mode will be considered, we only need to

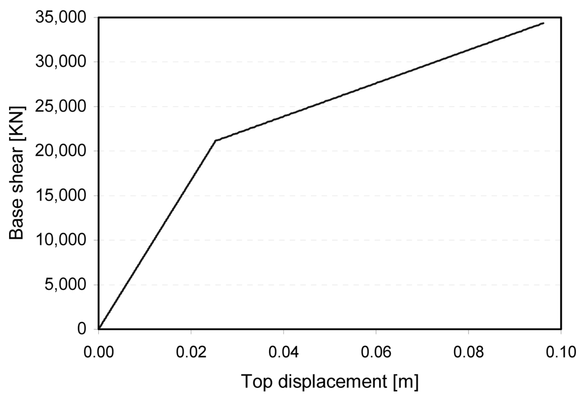


Fig. 8 Capacity curve for the first mode (tower without water)

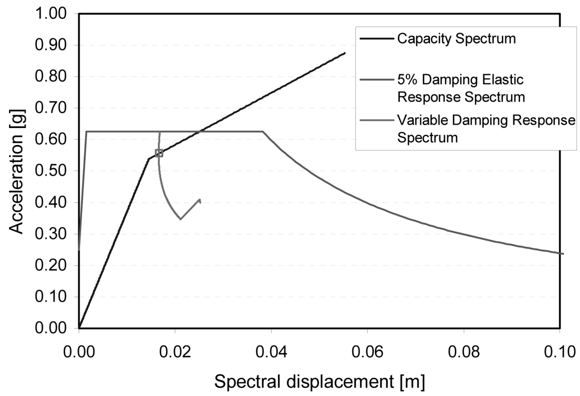


Fig. 9 Capacity spectrum, demand spectrum, and determination of the performance point for the first mode (tower without water)

Table 4 Modal and total performance points for the tower without water (multimodal CSM)

| | First mode | Second mode | Combined |
|---|---|---|---|
| $S_A$ [g] | 0.556 | 0.475 | 0.731 |
| $S_D$ [m] | 0.017 | 0.001 | 0.017 |
| $\Delta_{top}$ [m] | 0.029 | 0.001 | 0.029 |
| $V_b$ [KN] | 21,834 | 8,931 | 23,590 |

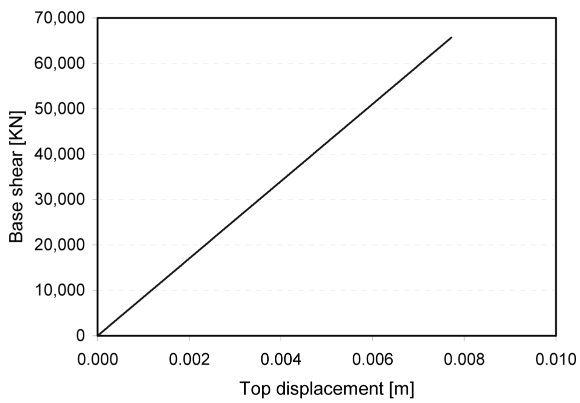


Fig. 10 Capacity curve for the second mode (tower without water)

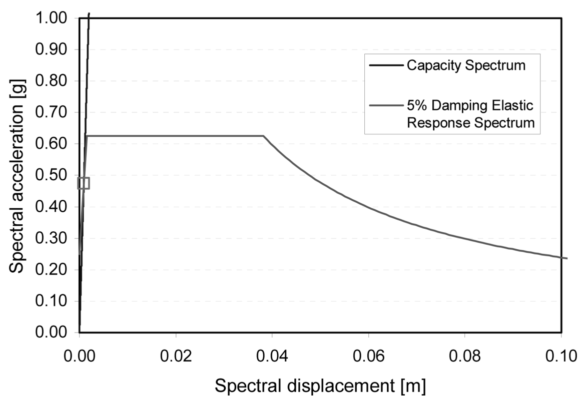


Fig. 11 Capacity spectrum, demand spectrum, and determination of the performance point for the second mode (tower without water)

apply the CSM to the second mode. The tower was then loaded with a force distribution pattern that follows the shape of the second mode. Except for the change in the load pattern, the procedure to obtain the pushover curve is the same as that for the conventional pushover analysis shown in Fig. 9. Fig. 10 shows the resulting pushover curve for the second mode load pattern. It can be seen that the pushover curve for this mode has no change in slope, i.e., the tower exhibits linear behavior.

To convert the pushover curve for the second mode into a capacity spectrum curve, the modal properties (modal participation factor, modal displacement of the top node, etc.) of the second mode are used. The resulting curve is shown in Fig. 11. This figure also shows the 5% elastic response spectrum in the acceleration-displacement format. In this case, the variable damping response spectrum was not needed because the structure behaves in a linear fashion. The performance point is simply the intersection of the linear capacity curve and the elastic spectrum.

Table 4 shows the coordinates $(S_A, S_D)$ of the performance point corresponding to the first and second modes. These two points are referred to as "modal" performance points. In addition, the table contains the corresponding coordinates $(V_b, \Delta_{top})$ of the pushover curve at the performance point, i.e., the physical inelastic response of the structure. These quantities are back-calculated using the same formulas to convert the pushover curve to capacity spectrum. The final performance point is obtained by combining the coordinates of the modal performance points according to the SRSS rule. The table shows the coordinates of the final performance point in the physical and modal domain for the tower when the surrounding and inside reservoir water is neglected.

### *5.4 Application of the adaptive CSM*

The application of the adaptive version of the CSM (Cocco 2004), which uses the "instantaneous" modal properties of the structure, is reported here. In this approach, the associated eigenvalue problem is solved whenever there is a change in the stiffness of the structure due to yielding, and the updated modal properties are used in the CSM. To separate out the different factors at play, the effects of the water are not included first. The results of the adaptive CSM are summarized in Table 5. The results in this table were obtained by applying the adaptive CSM to the first two modes of the tower and combining the results by means of the SRSS modal combination rule. The coordinates of the final performance point obtained are also shown in Table 5.

The displacement at the top of the tower with the adaptive multimodal CSM increased from 0.029 to 0.043 m, which represents an increase of almost 50% with respect to the standard multimodal CSM. The base shear force also increased from 23,590 to 26,011 kN, i.e., an increase of 10% with respect to the multimodal CSM. The first-mode results differ by similar quantities because the contribution of the second mode is not significant. It must be noticed also that since the response associated with the second mode does not enter into the post yielding range, the second-mode results obtained with the standard and adaptive CSM are identical.

It should be noticed that the proposed procedure has some similarities with a technique later proponed by Casarotti and Pinho (2007). However, the Casarotti and Pinho's technique employs the deformation pattern at each step to update an equivalent displacement of a single degree of freedom system. In our case, we use the first and second modes of the elastic structure but recalculated at each step after the nonlinear base spring reaches the yielding condition.

Table 5 Modal and total performance points for the tower without water (adaptive multimodal CSM)

| | First mode | Second mode | Combined |
|---|---|---|---|
| $S_A$ [g] | 0.506 | 0.475 | 0.694 |
| $S_D$ [m] | 0.025 | 0.001 | 0.025 |
| $\Delta_{top}$ [m] | 0.043 | 0.001 | 0.043 |
| $V_b$ [KN] | 24,429 | 8,931 | 26,010 |

Table 6 Comparison of results from the CSM (first three columns) and time history analyses (last three columns) for the tower without water

| Response | Conventional CSM | Multimodal CSM | Adaptive CSM | SAP2000 | RAM Performance | Matlab Program |
|---|---|---|---|---|---|---|
| $\Delta_{top}$ [m] | 0.029 | 0.029 | 0.043 | 0.028 | 0.027 | 0.028 |
| $V_b$ [KN] | 21,834 | 23,590 | 26,011 | 29,080 | 28,778 | 34,203 |

### 5.5 Comparison of CSM with nonlinear time history analysis

Although the Capacity Spectrum Method is considered an accepted technique for nonlinear static analysis, it is an approximate procedure and thus it is relevant to study the accuracy of its results before recommending its use for seismic analysis of a large inventory of intake structures. A time history analysis of the example tower was performed using two commercial structural analysis programs, SAP2000 (Computers and Structures 2004) and RAM Performance (RAM International 2004), and a Matlab-based program developed by the authors.

The results from the time history analyses (SAP2000, RAM and Matlab in-house program), along with those obtained with the CSM (conventional, multimodal and adaptive multimodal) are presented in Table 6. Recall that these results are applicable for a tower in dry conditions. The values of the response obtained from the three time history analyses agree well with each other, which is remarkable since each program uses different nonlinear models and integration schemes. The displacements predicted by the CSM approaches are similar to those obtained from the time history analyses, except for the multimodal adaptive CSM. The latter method yielded a peak displacement higher than the other CSM values. However, the peak base shear predicted by this method is closer to the values computed from the nonlinear dynamic analyses. In general, the CSM approaches led to smaller base shears than those predicted by the time history analyses. One possible reason for this difference could be that the higher modes have a non-negligible contribution to the shear force at the tower's base. Recall that only two modes were considered in the multimodal and adaptive CSM.

In summary, the results presented show that for the particular structural system considered, the multimodal CSM produces the most accurate results in terms of displacements, compared to those predicted by the time history analyses, whereas the adaptive CMS yields better results when the base shear is compared. These results need a word of caution: they are valid for the particular version of the adaptive CMS used in this work, and for the specific structure analyzed. For other structures, the literature on the subject indicates that, as it would be expected, it is the adaptive version the one that provides more accurate results.

### 5.6 Application of the CSM including hydrodynamic effects

The presence of the reservoir water surrounding and inside the tower is introduced in the CSM by means of the added masses procedure proposed by Goyal and Chopra (1989). The water-tower interaction effects were only evaluated for the multimodal CSM because this was the approach that produced the most accurate results for the tower without water. The pushover curve corresponding to the first mode is shown in Fig. 12, and is very similar to that obtained without the added masses (Fig. 8). The reason is that the only difference between the two analyses is the spatial variation of the applied loads, which follows the pattern of the first vibration mode corresponding to each case. The change in modal shape due to the additional masses is not significant because the masses are distributed proportional to the cross sectional dimensions and the stiffness properties of the structure are not altered. The first-mode capacity spectrum, shown in Fig. 13, exhibits more pronounced differences compared to the corresponding spectrum in which the hydrodynamic effects were ignored, because the capacity spectrum depends on three modal properties: the modal mass coefficient, the modal participation factor, and the modal component corresponding to the top displacement. In this figure the capacity spectrum is shown along with the elastic response spectrum and the variable damping curve. The performance point for this mode is represented by the intersection between the variable damping curve and the capacity spectrum.

The pushover curve obtained by applying an external loading pattern corresponding to the second mode is shown in Fig. 14. Here again the differences are minimal with the original pushover curve in Fig. 10, due to the same reasons stated before for the first mode case. Fig. 15 displays the

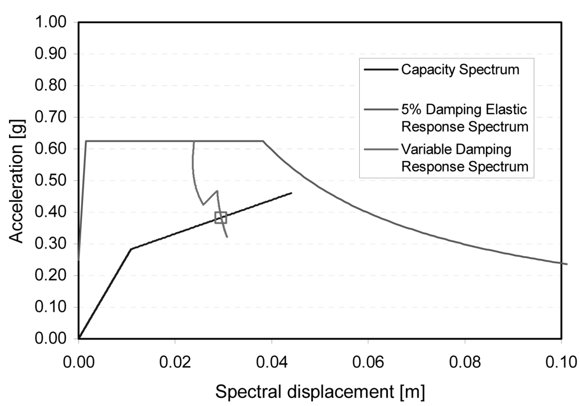


Fig. 13 Capacity spectrum, demand spectrum, and determination of performance point for the first mode (tower with water)

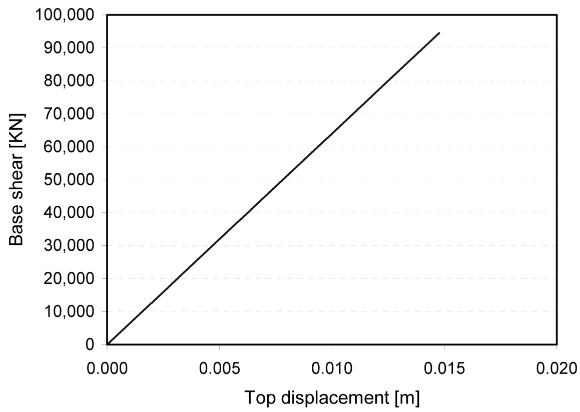


Fig. 14 Capacity curve for the second mode (tower with water)

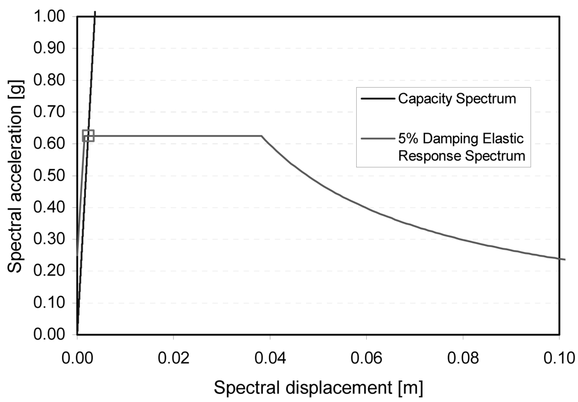


Fig. 15 Capacity spectrum, demand spectrum, and determination of the performance point for the 2nd mode (tower with water)

Table 7 Modal and total performance points for the tower with water (multimodal CSM)

| | First mode | Second mode | Combined |
|---|---|---|---|
| $S_A$ [g] | 0.383 | 0.625 | 0.733 |
| $S_D$ [m] | 0.030 | 0.002 | 0.030 |
| $\Delta_{top}$ [m] | 0.062 | 0.004 | 0.062 |
| $V_b$ [KN] | 33,397 | 24,334 | 41,322 |

Table 8 Comparison of results from the CSM and RSM analyses for the tower with water

| Response | Multimodal CSM | Multimodal CSM (linear) | RSM (USACE) |
|---|---|---|---|
| $\Delta_{top}$ [m] | 0.062 | 0.050 | 0.058 |
| $V_b$ [KN] | 41,322 | 59,751 | 59,646 |

capacity spectrum along with the linear elastic and variable damping spectra. Although there are some minor differences between the cases with and without added masses, in both situations the tower responds in the linear range.

The results obtained for this case are summarized in Table 7. The coordinates for the performance point are presented for each mode and the fourth column shows the coordinates obtained by combining the modal values. A notable increase in the response predicted by the multimodal CSM when the hydrodynamic effects are included can be observed. Compared with the results reported in Table 4 (in which the effect of the surrounding water was neglected), the top displacement increased by 114% and the base shear force by 75%. Clearly, regardless of whether the multimodal or the conventional CSM is used to obtain the nonlinear seismic response of the intake towers, it is vital to account for the effect of the inside and outside water.

Table 8 compares the CSM results with those obtained using the standard linear analysis procedure recommended in EM 1110-2-2400 (2003). This procedure is based on the response spectrum method and it takes into account the interaction between the tower and the outside and inside water. The table also shows the results obtained with the linear version of the CSM, in which the behavior of the structure is assumed to be entirely linear elastic. While the displacement response predicted by the multimodal CSM is larger than the linear response, the CSM results show a significant reduction in the base shear.

## 6. Conclusions

A methodology for the seismic analysis of intake towers based on different implementations of the Capacity Spectrum Method was presented. The structural nonlinear behavior was modeled by a nonlinear rotational spring located at the critical section. The corresponding moment-rotation curve was defined using an equivalent plastic hinge length calculated with a formulation proposed by Dove and Matheu (2005). To assess the accuracy of the CSM procedures, the results were compared with nonlinear time history analyses performed using two commercial and user-generated Matlab programs. The seismic input for the programs was an earthquake record compatible with a design spectrum. The response predicted by the conventional, multimodal and the adaptive CSM were similar and reasonably close to the nonlinear dynamic analyses, except that the adaptive CSM overestimated the displacements. However, the base shear predicted by the adaptive CSM was closer to those obtained from the time history analysis.

Another aspect of the seismic response of intake towers that was examined was the influence of the outside and inside water. It was previously reported that this effect was important for linear analyses and thus one of the objectives of the present study was to assess its importance to the nonlinear response. It was found that the response when the added hydrodynamic masses were included in the model was higher than when this effect was neglected. For the example considered in this study, the multimodal CSM predicted a top displacement 114% higher and a base shear 75% higher than those under empty reservoir conditions. The differences were due to changes in the capacity spectrum caused by the modification of the corresponding modal properties. Except for a small change in the relative values of the mass matrix used to calculate the lateral force distribution, the pushover curves were practically not altered. The multimodal CSM results were compared with the results obtained with the standard two-mode response spectrum procedure currently used for seismic design and evaluation of intake towers. The results highlight the potential for the CSM to become a very useful and effective tool for rapid evaluation of the nonlinear seismic response of intake towers.

The main contribution and the focus of the research undertaken was the inclusion of the external and internal added mass in a multimodal CSM which used the first two modes to calculate the capacity curve. An adaptive procedure was also applied, which is based on employing the updated mode shapes of the structure once the rotational base spring (representing the nonlinear behavior of the tower at its base) reaches the yielding level. Although there are a number of powerful adaptive pushovers proposed in the literature, we settled on the simple and straightforward procedure described before, because the main practical application of the entire method will be to asses the structural integrity of an inventory of intake towers.

## Acknowledgements

This work was sponsored by the Flood and Coastal Storm Damage Reduction Research Program of the Coastal and Hydraulics Laboratory, U.S. Army Engineer Research and Development Center in Vicksburg, Mississippi, USA, under the general supervision of Dr. Jack E. Davis, Technical Director, and Mr. Fred Pinkard, Program Manager. This study was performed as part of the efforts developed by the Geotechnical and Structures Laboratory under the Work Unit "Performance Evaluation and Rehabilitation of Semi-Embedded Appurtenant Structures," with Ms. Yazmin Seda-Sanabria as Work Area Leader and Dr. Enrique E. Matheu as Principal Investigator. Permission to publish was granted by Director, Geotechnical and Structures Laboratory, U.S. Army Engineer Research and Development Center.

## References

ACI Committee (1995), "307-98: Design and construction of reinforced concrete chimneys and commentary", American Concrete Institute, Farmington Hills, Michigan, USA.

Antoniou, S. and Pinho, R. (2004), "Advantages and limitations of adaptive and non-adaptive force-based

pushover procedures", *J. Earthq. Eng.*, **8**(4), 497-522.
Antoniou, S. and Pinho, R. (2004), "Development and verification of a displacement-based adaptive pushover procedure", *J. Earthq. Eng.*, **8**(5), 643-661.
ATC-40 (1996), "Seismic evaluation and retrofit of concrete buildings", Applied Technology Council, Redwood City, California, USA.
Aydinoğlu, M.N. (2003), "An incremental response spectrum analysis procedure based on inelastic spectral displacements for multi-mode seismic performance evaluation", *Bull. Earthq. Eng.*, **1**, 3-36.
Bracci, J.M., Kunnath, S.K. and Reinhorn, A.M. (1997), "Seismic performance and retrofit evaluation of reinforced concrete structures", *J. Struct. Eng.*, **123**(1), 3-10.
Casarotti, C. and Pinho, R. (2007), "An adaptive capacity spectrum method for assessment of bridges subjected to earthquake action", *Bull. Earthq. Eng.*, **5**(3), 377-390.
Chopra, A.K. and Goel, R.K. (2002), "A modal pushover analysis for estimating seismic demands for buildings", *Earthq. Eng. Struct. D.*, **31**, 561-582.
Cocco, L.J. (2004), "Evaluation of the nonlinear seismic response of intake and control towers with the capacity spectrum method", MSc. Dissertation, December de 2004. Mayagüez, Puerto Rico.
Computers & Structures, Inc. (2004), "SAP2000: Integrated software for structural analysis & design", Berkeley, California, USA.
Dove, R.C. and Matheu, E.E. (2005), "Ultimate deflection capacity of lightly reinforced concrete intake towers," *ACI Struct. J.*, **102**(2), 214-223.
Fajfar, P. (1999), "Capacity spectrum method based on inelastic demand spectra", *Earthq. Eng. Struct. D.*, **28**, 979-993.
Fajfar, P. and Dolsek, M. (2001), "A transparent nonlinear method for seismic performance evaluation", Implications of Recent Earthquakes on Seismic Risk, Imperial College Press, London, UK.
Freeman, S.A., Nicoletti, J.P. and Tyrell, J.V. (1975), "Evaluations of existing buildings for seismic risk – a case study of puget sound naval shipyard bremerton, washington", *Proceedings of the 1st U.S. National Conference on Earthquake Engineering*, EERI, Berkeley, California.
Freeman, S.A. (1978), "Prediction of response of concrete buildings to severe earthquake motion", *Douglas McHenry International Symposium on Concrete and Concrete Structures*, SP-55, American Concrete Institute, Detroit, Michigan, USA.
Freeman, S.A. (1987), "Code designed steel frame performance characteristics", *Dynamics of Structures, Proceedings of the 1987 Structures Congress*, American Society of Civil Engineers, Orlando, Florida.
Freeman, S.A. (1992), "On the correlation of code forces to earthquake demands", *Proceedings of the 4th U.S./Japan Workshops on Improvement of Building Structural Design and Construction Practices*, ATC 15-3, Applied Technology Council, Kailua-Kona, Hawaii, USA.
Goyal, A. and Chopra, A.K. (1989), "Simplified evaluation of added hydrodynamic mass for intake towers", *J. Eng. Mech.*, **115**(7), 1393-1435.
Gupta, B. and Kunnath, S.K. (2000), "Adaptive spectra-based pushover procedure for seismic evaluation of structures", *Earthq. Spectra*, **16**(2), 367-392.
Isakovic, T. and Fischinger, M. (2006), "Higher modes in simplified inelastic seismic analysis of single column bent viaducts", *Earthq. Eng. Struct. D.,* **35**(1), 95-114.
Kalkan, E. and Kunnath, S.K. (2006), "Adaptive modal combination for nonlinear static analysis of building structures", *J. Struct. Eng.*, **132**(11), 1721-1731.
Kowalsky, M.J., Priestley, M.J.N. and MacRae, G.A. (1994), "Displacement-based design, a methodology for seismic design applied to SDOF reinforced concrete structures", Report SSRP-94/16, Structural System Research Project, University of California, San Diego, La Jolla, California, USA.
Krawinkler, H. and Seneviratna, G.D.P.K. (1997), "Pros and cons of a pushover analysis of seismic performance evaluation", *Eng. Struct.*, **20**(4), 452-464.
Liaw, C.Y. and Chopra, A.K. (1974), "Dynamics of towers surrounded by water", *Earthq. Eng. Struct. D.*, **3**, 33-49.
Lin, Y.Y. and Chang, K.C. (2003), "An improved capacity spectrum method for ATC-40", *Earthq. Eng. Struct. D.*, **32**, 2013-2025.
Lupoi, A., Franchin, P. and Pinto, P.E. (2007), "Further probing of the suitability of pushover analysis for the

seismic assessment of bridge structures", *Proceedings of the First US-Italy Workshop on Seismic Design of Bridges,* Pavia, Italy.
Mahaney, J.A., Paret, T.F., Kehoe, B.E. and Freeman, S.A. (1993), "The capacity spectrum method for evaluating structural response during the Loma Prieta earthquake", *Proceedings of the National Earthquake Conference*, Memphis, Tennessee, USA.
Newmark, N.M. and Hall, W.J. (1982), "Earthquake spectra and design", EERI Monograph Series, Earthquake Engineering Research Institute, Oakland, California, USA.
Paraskeva, T., Kappos, A. and Sextos, A. (2006), "Extension of modal pushover analysis to seismic assessment of bridges", *Earthq. Eng. Struct. D.,* **35**(10), 1269-1293.
Pyle, S.L. and Morris, G.R. (2001), "Pushover analysis: a tool for performance based design", *Struct. Eng.*, March, 28-33.
RAM International (2004), *RAM Perform-3D*, Carlsbad, California, USA.
Suarez, L.E. and Montejo, L.A. (2005), "Generation of artificial earthquakes via the wavelet transform", *Int. J. Solids Struct.*, **42**(21-22), 5905-5919.
Suarez, L.E. and Montejo, L.A. (2007), "Applications of the wavelet transform in the generation and analysis of artificial accelerograms", *Struct. Eng. Mech.*, **27**(2), 173-197.
U.S. Army Corps of Engineers (2003), "Structural design and evaluation of outlet works", Engineer Manual No. 1110-2-2400, Department of the Army, U.S. Army Corps of Engineers, Washington, DC, USA.